IEEE Open Access Journal of
Power and Energy

Received 17 July 2023; revised 10 October 2023; accepted 8 November 2023. Date of publication 13 November 2023;
date of current version 20 November 2023.

Digital Object Identifier 10.1109/OAJPE.2023.3332227

An RMRAC With Deep Symbolic Optimization for DC–AC Converters Under Less-Inertia Power Grids

**GUILHERME VIEIRA HOLLWEG[1] (Member, IEEE), VAN-HAI BUI[1] (Member, IEEE),
FELIPE LENO DA SILVA[2], RUBEN GLATT[2] (Member, IEEE),
SHIVAM CHATURVEDI[1] (Member, IEEE), AND WENCONG SU[1] (Senior Member, IEEE)**

[1]Department of Electrical and Computer Engineering (ECE), University of Michigan-Dearborn, Dearborn, MI 48128 USA
[2]Lawrence Livermore National Laboratory, Livermore, CA 94550 USA

CORRESPONDING AUTHOR: W. SU (wencong@umich.edu)

The work of Guilherme Vieira Hollweg, Van-Hai Bui, and Wencong Su was supported in part by the U.S. National Science Foundation under Grant 2321661. The work of Felipe Leno da Silva and Ruben Glatt was supported in part by the U.S. Department of Energy by Lawrence Livermore National Laboratory under Contract DE-AC52-07NA27344 and in part by the Lawrence Livermore National Security under Grant LLC. LLNL-JRNL-848300.

ABSTRACT This paper presents a novel approach for grid-injected current control of DC-AC converters using a robust model reference adaptive controller (RMRAC) with deep symbolic optimization (DSO). Grid voltages are known to be time-varying and can contain distortions, unbalances, and harmonics, which can lead to poor tracking and high total harmonic distortion (THD). The proposed adaptive control structure addresses this issue by enabling or disabling harmonics compensation blocks based on the grid voltage's characteristics. The DSO framework is implemented to generate an equivalent mathematical expression of the grid voltages, which is then incorporated into the RMRAC-based controller. The controller is then able to reconfigure itself to adequately compensate for high harmonics present in the grid, reducing computational complexity and improving performance. A controller-hardware-in-the-loop (C-HIL) environment with a Typhoon HIL 604 and a TSM320F28335 DSP is implemented to demonstrate that the proposed RMRAC-based structure with DSO outperforms both the same adaptive structure without DSO and a superior RMRAC-based controller. The proposed approach has potential applications in less-inertia power grids, where efficient and accurate control of grid-connected converters is crucial.

INDEX TERMS Grid-connected converters, LCL filter, deep symbolic optimization, RMRAC, harmonics compensation, C-HIL.

I. INTRODUCTION

IN RECENT years, traditional power generation systems have been replaced by renewable energy systems (RES) in an effort to reduce the global warming and pollution associated with fossil fuels [1]. Power electronics by means of grid-connected converters (GCCs) are an important part of modern power systems, and their stability is critical to ensure the safety and reliability of the power grid [2].

The controllers of power electronics systems play a vital role in maintaining grid stability. Regarding DC-AC power converters, control structures for GCCs typically involve a feedback loop that continuously adjusts the system's parameters to maintain stable operation. Usually, when an inverter-based structure is designed, it takes into consideration the dynamics variation from the primary source and the unpredictability of the grid, as well as pulse-width modulation (PWM) switching harmonics suppression (by means of output filters), system damping, and DC-bus voltage control, among others [3], [4]. However, stability issues in control structures for GCCs are particularly acute in less-inertia power grids. Weak grids are characterized by low short-circuit capacity and high electrical impedance, which can lead to voltage fluctuations and reduced stability. In contrast, very weak grids have even lower short-circuit capacity and higher impedance, making them more challenging to operate in a stable manner [5], [6]. Since the main grid voltages and their behavior cannot be controlled by RES grid-connected structures, which usually present the grid voltages as references for injecting power into the system, grid uncertainty poses a great challenge for the control of inverter-based structures.

Various types of output filters have been studied to reduce harmonic components generated by the converter's switching action, with L and LCL filters being the most common for GCCs [7]. The LCL filter offers greater suppression of harmonics at high frequencies, along with cost reduction and smaller size and weight. However, the LCL filter is more complex in terms of modeling, design, and control challenges due to its significant resonance peak [7], [8]. To attenuate this peak, passive and active damping approaches are available. Passive damping is a method of reducing the resonance peak of output filters by adding other elements to the filters through hardware [9], [10]. For the LCL filter, a common approach is to insert a resistor in series with the filter capacitor, which has less current circulation and leads to less power dissipation in the form of heat. On the other hand, active damping is typically performed through software by the control system. Although there is no reduction in the system's efficiency, the complexity of the control structure tends to be increased [11], [12]. Several standards, including IEEE 519 [13] and IEEE 1547 [14], impose restrictions on energy quality and the total harmonic distortion (THD) rate of grid-side currents.

For less-inertia power grids, i.e., those with high penetration of inverter-based resources, the control design tends to be a challenging task. In these types of grids, power electronics systems can cause significant stability issues, including voltage flicker, resonance, and oscillations [15]. To mitigate these issues, control structures for power electronics systems must be designed to account for the unique characteristics of these grids. Regarding current control of GCCs, several controllers have been proposed: multi-resonant structures [16], [17] as well as model predictive controllers (MPC) have recently demonstrated high efficiency in controlling the currents of grid-tied inverter-based structures [18], [19]. However, multi-resonant controllers have a fixed range of stability margins, while MPC structures, even those that are adaptive, as [20] and [21], use a predictive model of the system's behavior to calculate the optimal control inputs that will maintain stability. For this task, the plant model needs to be very accurate.

Considering grids that can change their behavior from strong to weak or to very weak and present several disturbances as well as strong harmonics, a fixed gains structure may not be sufficient to maintain system stability [6]. If the GCC is not capable of keeping the currents well regulated, it tends to disconnect from the grid, which may affect RES grid stability. Under these circumstances, adaptive controllers tend to be a good choice for this kind of system because they can change the values of their gains in response to perturbations, which can be parametric variations, matched or unmatched dynamics, and exogenous disturbances [22], [23]. Moreover, they need to be mathematically robust, ensured by means of Lyapunov stability analysis. In the recent past, robust model reference adaptive controllers (RMRAC)-based systems emerged as suitable alternatives for current control of GCCs with LCL filters [12], [24], [25], [26] and obtained good performance and robustness to several disturbances, unmodeled dynamics, and even very weak grids [6]. However, these RMRAC-based structures usually present additional features to deal with disturbances and unmodeled dynamics in order to improve the controller performance. These features tend to increase the mathematical complexity and the computational burden, which is an important topic for control applications using digital signal processors (DSP), since they usually have limited memory.

This paper presents a new RMRAC-based adaptive control structure for current control of GCCs with LCL filters, with adaptive selective harmonics compensation featuring a novel approach for voltage prediction based on the deep symbolic optimization (DSO) framework [27], [28], [29]. Since learning-based techniques normally produce high computational demand, the aim of this research is to use DSO not in real time but in windows of time (every few minutes), giving an evaluation that is performed offline and feeding the controller structure back to be reorganized properly as soon as the regression is done. The controller enables and disables harmonics compensation according to necessity, becoming a reconfigurable direct adaptive controller, which alleviates the computational burden and reduces the controller's complexity.

The contributions of the paper can be outlined as follows:

- we define a novel approach for adaptive current control based on symbolic optimization to quickly obtain equivalent mathematical expressions of the grid voltage of a single-phase GCC to predict the voltages at the point of common coupling (PCC) to dynamically reorganize the controller structure and gains in order to keep the system stable and well regulated, even in scenarios with severe distortion and harmonic content;
- we show that our enhanced RMRAC-based structure is able to control the behavior of the entire system given the dynamic status and unpredictability of the grid voltages, improving system power quality and stability.

Moreover, an evaluation is provided of hardware-in-the-loop results comparing the proposed controller with a standard RMRAC and a RMRAC-ASTSM structure [12]. It is also important to highlight that since the harmonics compensation is implemented by means of periodic disturbances compensation, this technique could also be applied to other direct adaptive structures, as those [3], [6], [24], [25], [26].

The remainder of this work is organized as follows: Section II discusses the plant, and Section III presents the RMRAC-based controller design. Section IV describes the DSO tuning. Section V shows the results obtained with a 2.7 kW single-phase GCC with an LCL filter. Finally, Section VI gives the final considerations of this study.

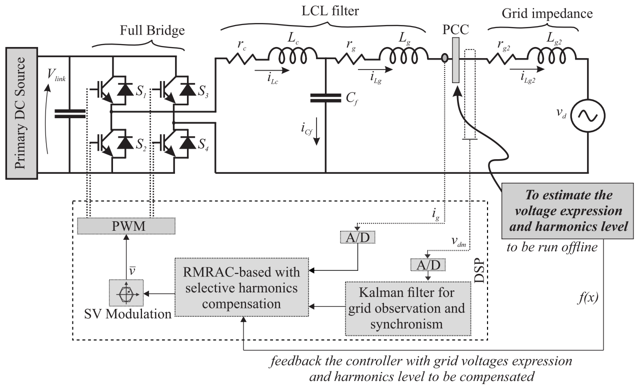

FIGURE 1. Single-phase DC-AC converter and control structure schematic.

II. VOLTAGE SOURCE INVERTER WITH LCL FILTER

A. PLANT DESCRIPTION

Even though three-phase DC-AC converters are more common for grid-connected applications, a case study of a single-phase converter was chosen, for simplicity. Furthermore, to extend the analysis from single-phase to three-phase converters, a few steps are needed to decouple $\alpha\beta$ models with respect to abc, as explained in [3]. The electrical circuit diagram of the single-phase grid-tied voltage source inverter (VSI) with LCL filter is depicted in Fig. 1. In this diagram, r_c and L_c represent the inverter-side impedance, r_g and L_g represent the grid-side impedance, and C_f is the LCL filter capacitor. In addition, the grid impedance is composed of L_{g2} and r_{g2}, which are usually unknown in practical applications. The grid voltage and primary DC source are represented by v_d and V_{link}, respectively, while the measured phase voltage and current are denoted by v_{dm} and i_g, respectively. The modeling of the grid-tied VSI with LCL filter is extensively discussed in [12] and [26] and therefore will not be covered in this manuscript. Note that the DSO technique is applied to the grid voltage dataset read at the PCC. In this way, the grid information obtained from the equivalent mathematical expression of the grid voltages serves as feedback to the current control structure algorithm.

Based on the equivalent circuit of the LCL filter presented in [12] and [30], the transfer function relating the modulated voltage synthesized by the voltage source inverter (VSI) and the grid-injected currents can be obtained using Kirchhoff's circuit laws and state-space modeling. Thus, the LCL transfer function for current control can be expressed as follows:

$$\frac{i_g(s)}{\bar{v}(s)} = \frac{b_0}{s^3 + a_2 s^2 + a_1 s + a_0}, \tag{1}$$

where $\bar{v}$ is the inverter voltage, synthesized through the modulation technique. Moreover, $b_0 = \frac{1}{L_g L_c C_f}$, $a_2 = \frac{(R_g L_c + R_c L_g)}{L_g L_c}$, $a_1 = \frac{(L_c + L_g + R_g R_c C_f)}{L_g L_c C_f}$, and $a_0 = \frac{R_g + R_c}{L_g L_c C_f}$. More details about LCL filter modeling can be seen in [12] and [26].

B. PLANT PARAMETERS

The design of the LCL elements was made according to [30]. The obtained values for the output filter were $L_c = 1.7\ mH$, $C_f = 25\ \mu F$, and $L_g = 0.45\ mH$, considering $r_c = r_g = 50\ m\Omega$. Additionally, the power inverter is $P_{in} = 2700\ W_{pk}$. Moreover, the considered DC voltage is $V_{link} = 400\ V$, and grid parameters are unknown since they vary according to the local grid characteristics [3]. In addition, the switching frequency and sampling period are $f_s = 5.04\ kHz$ and $T_s = 198.4\ \mu s$, respectively. To synchronize the inverter with the electrical grid, a Kalman filter-phase locked loop (KF-PLL) was implemented [31]. Lastly, the control action, u, is synthesized by space vector modulation, as presented in [32].

The transfer function $G(z)$ of the discrete-time LCL filter (with 1-sample time delay) can be obtained by placing the converter parameters into (1) and discretizing it using the zero-order hold (ZOH) method with a sampling time of $T_s = 198.4\ \mu$s, resulting in

$$G(z) = \frac{i_g(z)}{\bar{v}_{ab}(z)} = \frac{d_2 z^2 + d_1 z + d_0}{z(c_3 z^3 + c_2 z^2 + c_1 z + c_0)}, \tag{2}$$

where $d_2 = 0.0541323$, $d_1 = 0.166996$, $d_0 = 0.053363$, $c_3 = 1$, $c_2 = 0.01586$, $c_1 = -0.01590$, and $c_0 = -0.9725$.

III. ADAPTIVE CONTROLLER

In this section, the RMRAC-based controller and reference model design are introduced for regulating the grid-injected currents in a single-phase VSI with LCL filter. The general model of the plant can be written as

$$G(z) = G_0(z)[1 + \mu\Delta_m(z)] + \mu\Delta_a(z), \tag{3}$$

where $\mu\Delta_m$ and $\mu\Delta_a$ are unmodeled multiplicative and additive dynamics, respectively. The modeled part of the plant is described as

$$G_0(z) = k_p \frac{Z_p(z)}{R_p(z)}. \tag{4}$$

G_0 must fulfill specific requirements, which are listed as follows:

A1) The high gain signal k_p must be known.

A2) $Z_p(z)$ and $R_p(z)$ must be monic polynomials of degree m and n, respectively.

A3) $Z_p(z)$ must be a Schur polynomial.

A4) $\Delta_m(z)$ must be a Schur transfer function and $\Delta_a(z)$ must be a strictly proper Schur transfer function.

A5) The stability margin of addictive dynamics $\Delta_a(z)$ and multiplicative dynamics $\Delta_m(z)$ must have a lower bound that is known.

Note that these assumptions are usual in RMRAC-based structures. In addition, the satisfaction of these assumptions for LCL filters was discussed in [12], which leaded to a reduced order reference model design.

The general equation that describes the reference model is

$$W_m(z) = \frac{k_m}{R_m(z)}, \tag{5}$$

and it is subject to the following assumption:

A6) $R_m(z)$ is a monic polynomial of order $(n - m)$ (the same relative degree of $G_0(z)$), with all roots inside the unit circle and k_m is a constant with the same sign as k_p.

Since the reference model of (5) is chosen by the designer, A6 can be met. However, for this application, given that the plant is relative degree $n^* = 3$, a reduced-order model of the plant is considered for designing the reference model, $n^* = 1$. Reduced-order modeling of systems is a common approach in adaptive controllers, as [6], [12], [22], [23], [24], and [33], and it will be better addressed in the next Section.

A. RMRAC-BASED STRUCTURE

The control action is determined from

$$\boldsymbol{\theta}^T(k)\boldsymbol{\omega}(k) + r(k) = 0, \tag{6}$$

where the reference signal is denoted by $r(k)$, the adaptive gains vector is represented by $\boldsymbol{\theta}(k)$, and the regressor vector is given by $\boldsymbol{\omega}(k)$. The regressor vector $\boldsymbol{\omega}(k)$ comprises four components: $\boldsymbol{\omega}_1(k)$, $\boldsymbol{\omega}_2(k)$, $y(k)$, and $u(k)$, arranged in a vertical structure. The two reconstructive filters $\boldsymbol{\omega}_1(k)$ and $\boldsymbol{\omega}_2(k)$ have specific structures, as

$$\begin{aligned}\boldsymbol{\omega}_1(k+1) &= (\boldsymbol{I} + \boldsymbol{F}T_s)\boldsymbol{\omega}_1(k) + \boldsymbol{q}u(k),\\ \boldsymbol{\omega}_2(k+1) &= (\boldsymbol{I} + \boldsymbol{F}T_s)\boldsymbol{\omega}_2(k) + \boldsymbol{q}y(k),\end{aligned} \tag{7}$$

where $\boldsymbol{I}$ is an $n \times n$ identity matrix while $(\boldsymbol{F}, \boldsymbol{q})$ is a pair that is controllable. The matrix $\boldsymbol{F}$ is stable, and the parameter vector $\boldsymbol{q}$ is controllable, with dimensions of $n_p - 1 \times n - 1$ and $n - 1$, respectively [34]. Moreover, as previously mentioned, T_s represents the sampling time.

Observe that (6) and (7) are general representations for RMRAC structures. However, for the grid-connected current control with LCL filter addressed in this work, the nominal part of the plant is a first-order transfer function. In this setup, the computation of $\boldsymbol{\omega_1}$ and $\boldsymbol{\omega_2}$ is unnecessary. Hence, $\boldsymbol{\theta}^T(k) = [\ \theta_1(k)\ \theta_2(k)\ ]$ and $\boldsymbol{\omega}(k) = [\ u_r(k)\ y(k)\ ]$. Expanding (6) considering the first-order $G_0(z)$ and $W_m(z)$,

$$\theta_1(k)u_r(k) + \theta_2(k)y(k) + r(k) = 0, \tag{8}$$

and performing the proper multiplications and rearranging the terms, we have

$$u_r(k) = \frac{-\theta_2(k)y(k) - r(k)}{\theta_1(k)}, \tag{9}$$

which is the implementable form of the adaptive control action. The algorithm employed for adapting the parameters is the gradient algorithm [12], [34], as

$$\boldsymbol{\theta}(k+1) = \boldsymbol{\theta}(k) - T_s\sigma(k)\boldsymbol{\Gamma}\boldsymbol{\theta}(k) - T_s\,\kappa\,\frac{\boldsymbol{\Gamma}\boldsymbol{\zeta}(k)\epsilon(k)}{\bar{m}^2(k)}, \tag{10}$$

where the augmented error at time instant k is

$$\epsilon(k) = e_1(k) + \boldsymbol{\theta}^T(k)\boldsymbol{\zeta}(k) - y_m(k), \tag{11}$$

and the auxiliary vector $\boldsymbol{\zeta}$ is

$$\boldsymbol{\zeta} = W_m(z)\boldsymbol{\omega}. \tag{12}$$

Observe that (11) is the implementable form of the augmented error. The deduction for obtaining ϵ is fully presented in [34] and [35].

The tracking error $e_1(k)$ is defined as the difference between the plant output and the reference model output, as $e_1(k) = y(k) - y_m(k)$. The vector $\boldsymbol{\zeta}(k)$ corresponds to the reference-model filtered vector $\boldsymbol{\omega}(k)$ using $W_m(z)$. To ensure that all closed-loop signals are bounded, the majorant signal [34], [35] is given by

$$\bar{m}^2(k) = m^2(k) + \boldsymbol{\zeta}^T(k)\boldsymbol{\Gamma}\boldsymbol{\zeta}(k), \tag{13}$$

where

$$m(k+1) = (1 - T_s\delta_0)m(k) + T_s\delta_1(1 + |u(k)| + |y(k)|), \tag{14}$$

where the conditions for the parameters $m(0)$, δ_0, δ_1, and p_0 are as follows: $m(0) > \delta_1/\delta_0$ and $\delta_0 + \delta_1 \leq \min[p_0, q_0]$, where $\delta_1 > 0$ and $q_0 > 0$. Additionally, the poles of $W_m(z - q_0)$ and the eigenvalues of $F + q_0\boldsymbol{I}$ should be stable. Moreover, $0 < p_0 < 1$, which is a known lower bound on the stability margin of p, where p represents the poles of $\Delta_m(z-p)$ and $\Delta_a(z - p)$ is stable [34], [35].

The matrix $\boldsymbol{\Gamma}$ is a positive definite symmetric matrix of size $n \times n$, which governs the rate of parametric convergence. The choice of this matrix is relatively flexible since it contributes to the majorant signal. However, to speed up the parametric convergence, a positive scaling factor κ is introduced in (10). The values of the parameters related to the convergence rate can be selected arbitrarily, as long as $\Gamma\kappa T_s \leq 20$ [23], [34]. Generally, a higher value of κ results in a faster tracking response. Additionally, the gradient algorithm incorporates a σ-modification to enhance its robustness and prevent parameters drifting [34], [36]. The σ-modification is computed as follows:

$$\sigma(k) = \begin{cases} 0 & \text{if } \|\boldsymbol{\theta}(k)\| < M_0 \\ \sigma_0\left(\dfrac{\|\boldsymbol{\theta}(k)\|}{M_0} - 1\right) & \text{if } M_0 \leq \|\boldsymbol{\theta}(k)\| < 2M_0, \\ \sigma_0 & \text{if } \|\boldsymbol{\theta}(k)\| \geq 2M_0 \end{cases} \tag{15}$$

where $M_0 > \|\boldsymbol{\theta}^*\|$ is the upper limit of $\boldsymbol{\theta}(k)$ norm, oversized due to lack of knowledge of $\|\boldsymbol{\theta}^*\|$, and σ_0 is the maximum value of the modification function [25], [35].

B. ELECTRICAL GRID VOLTAGE DISTURBANCE REJECTION

As shown in (1), the LCL model does not account for the dynamics of the electrical grid. However, it can be treated as an external periodic disturbance [3], [12]. Thus, to handle this disturbance, a control action needs to be added to (9), as

$$u_d(k) = -\frac{\theta_c(k)}{\theta_1(k)}V_c(k) - \frac{\theta_s(k)}{\theta_1(k)}V_s(k), \tag{16}$$

where the adaptive gains $\theta_c(k)$ and $\theta_s(k)$ are used to compensate for the phase $V_s(k)$ and quadrature $V_c(k)$, respectively,

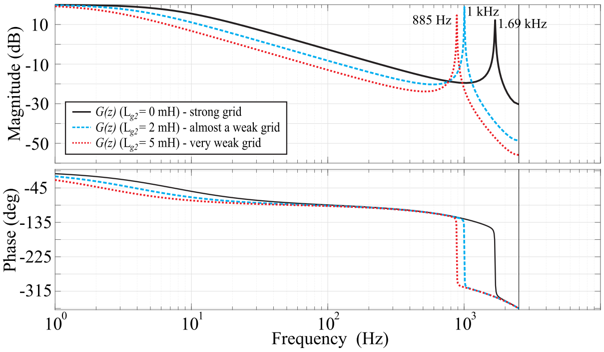

FIGURE 2. ***G*(*z*) Bode diagram with multiples values of L_{g2}.**

of the electrical grid voltage. The signals $V_s(k)$ and $V_c(k)$ represent the sinusoidal components of the grid fundamental harmonics and are given by $V_s(k) = \sin(2\pi f k T_s)$ and $V_c(k) = \cos(2\pi f k T_s)$, where f is the frequency of the electrical grid and T_s is the sampling period.

Thus, the complete control action for grid-side current regulation of a grid-tied power converter with RMRAC structure is obtained by summing the individual control actions, which were given before. Then, it is possible to obtain a new expression for the complete control action

$$u(k) = u_r(k) + u_d(k). \tag{17}$$

More details about the grid voltage being considered as a periodic exogenous disturbance can be read in [3], [12], and [25].

C. MODEL REFERENCE DESIGN

To reduce the complexity of the adaptive control structure, which is directly related to the relative degree of the reference model, a reduced-order model of the LCL filter is considered, as both the original plant and the reference model must have the same relative degree. This kind of approach is common in direct adaptive controllers design, as discussed extensively in [23]. The simplified model should consider the dynamics only at frequencies of interest, typically the low frequencies for this application, similar to the original plant. Therefore, the resonance peak of the LCL filter, which is close to the Nyquist frequency, is disregarded in the simplified model, since it is located at a high frequency. Fig. 2 shows the Bode diagram of the discrete-time plant, when considering grid inductance values such as $L_{g2} = 0$ mH (SCR = 35.21), $L_{g2} = 2$ mH (SCR = 6.47) and $L_{g2} = 5$ mH (SCR = 2.91).

Note that as the grid inductance increases, the plant gradually becomes more difficult to control, as its dynamics drastically change and its margins decrease, tending to require more robustness from the control algorithm to keep the closed-loop system stable. Additionally, it can be observed that the resonance peak of the system shifts toward the low frequencies. The plant frequency response under a very strong grid ($L_{g2} = 0$ mH) presented a resonance peak at 1.69 kHz, while under a very weak grid ($L_{g2} = 5$ mH), it was at 885 Hz. A resonance peak closer to low frequencies may characterize a serious problem, since maintaining the proper functioning of the system requires $10 f_g < f_{res} < 0.5 f_s$, where f_g is the grid frequency, f_{res} the resonance frequency of the LCL filter, and f_s is the switching frequency [30].

For control design, a reduced-order model from $G(z)$ is considered, disregarding the pair of complex conjugated poles that create the resonance peak. The reduced model is

$$G_0(z) = \frac{0.09186}{(z - 0.9908)}, \tag{18}$$

where G_0 represents the reduced-order plant model, which should accomodate A1)-A5), previously presented in Section III.

Thus, since the reduced-order plant model has a relative degree of one, the reference model must be also $n^* = 1$ to attend the matching condition [34], [35]. The designed model reference is

$$W_m(z) = \frac{0.7246}{(z - 0.2754)}. \tag{19}$$

The mathematical procedure for the LCL simplification is similar to what is presented in [12], and more details about reference model design can be found in [12] and [26].

D. SELECTIVE HARMONICS COMPENSATION

To synchronize with the grid voltage, the Kalman filter-PLL from [31] is employed. The filter estimates the grid voltage by processing the sine and cosine signals of the fundamental component of v_d (60 Hz). By performing some mathematical operations, multiple harmonic components of the fundamental frequency, such as the 2^{nd} (120 Hz), 3^{rd} (180 Hz), 5^{th} (300 Hz), 7^{th} (420 Hz), and so on, can be generated in the control algorithm. Consequently, the control law can be rewritten to compensate for these harmonics, for example by considering the 5^{th} and 7^{th} harmonics and rewriting the control law as

$$\bar{\boldsymbol{\theta}}^T(k)\bar{\boldsymbol{\omega}}(k) + r(k) = 0, \tag{20}$$

where the gain vector, $\bar{\boldsymbol{\theta}}$, is

$$\begin{aligned}\bar{\boldsymbol{\theta}}^T &= [\ \theta_1(k)\ \theta_2(k)\ \theta_c(k)\ \theta_s(k)\ \theta_{c5^{th}}(k)\ \theta_{s5^{th}}(k)\\ &\qquad \theta_{c7^{th}}(k)\ \theta_{s7^{th}}(k)\ ],\end{aligned}$$

and the parameter vector, $\bar{\boldsymbol{\omega}}$, is

$$\begin{aligned}\bar{\boldsymbol{\omega}}^T &= [\ u(k)\ y(k)\ V_c(k)\ V_s(k)\ V_{c5^{th}}(k)\ V_{s5^{th}}(k)\\ &\qquad V_{c7^{th}}(k)\ V_{s7^{th}}(k)\ ].\end{aligned}$$

By expanding the terms of (20) and following the steps discussed in Section III-A, we can express the control action with harmonic compensation rewriting (17), as:

$$u(k) = u_r(k) + u_d(k) + u_{d5^{th}}(k) + u_{d7^{th}}(k), \tag{21}$$

where $u_r(k)$ and $u_d(k)$ were presented earlier and are not modified. Moreover, $u_{d5^{th}}(k) = \frac{-\theta_{c5^{th}}(k)V_{c5^{th}}(k) - \theta_{s5^{th}}(k)V_{s5^{th}}(k)}{\theta_1(k)}$ and $u_{d7^{th}}(k) = \frac{-\theta_{c7^{th}}(k)V_{c7^{th}}(k) - \theta_{s7^{th}}(k)V_{s7^{th}}(k)}{\theta_1(k)}$.

The above control law presented in this work guarantees global stability since the harmonic components are limited by a majorant signal that ensures the boundedness of all closed-loop signals and is adapted at each iteration by the adaptation algorithm. This approach is similar to the one proposed in [12], where the grid disturbance rejection terms were estimated from the KF-PLL and dealt with proper adaptive control contributions from MRAC. However, in this work, additional harmonic compensation is provided from this disturbance-rejection control term. Therefore, the global stability of the controller is maintained, and the same controller constraints as discussed in [23] and [34] are still valid.

The selective harmonics compensation, in this case of the 5^{th} and 7^{th} orders, tends to increase the computational burden of the adaptive control structure, since there is the addition of 4 adaptation gains, 2 of them for each compensated component. If compensations for the 2^{nd}, 3^{rd}, 11^{th}, and 13^{th} orders are considered, for example, 8 additional parameters have to be included in the control algorithm, becoming 12 in total for only selective harmonics compensation (plus 4 from the reference model and 2 from fundamental grid compensation), making the structure unfeasible for most commercial DSPs since it would take too much calculation and require too much memory from the microcontroller to process the equations in one sampling time T_S. However, by using the DSO to take advantage of the harmonics to be compensated for according to necessity, this unfeasibility is eliminated. It is possible to obtain an RMRAC-based controller to compensate for only the most significant harmonics in the grid, once equations (20)–(21) can be updated accordingly. This strategy brings to the table a reconfigurable RMRAC-based structure that implements multi-harmonics compensation but enables and disables the corresponding compensations depending on the grid behavior (to be given feedback by the DSO). Fig. 3 presents the general block diagram of the RMRAC-based control structure.

Moreover, this reconfigurable technique presented in this section can be expanded to other direct adaptive structures and applications. However, the complexity of the system and whether it is implementable in the available microcontroller must be taken into consideration for each particular case.

IV. DEEP SYMBOLIC OPTIMIZATION FOR GRID VOLTAGES REGRESSION

Deep symbolic optimization (DSO) is the state-of-the-art technique for performing symbolic optimization. DSO can discover mathematical expressions from data by using a specific dataset and several tokens in a library (predefined by the user), in which a learning-based model tries to obtain the equivalent mathematical expression that better fits the provided dataset. DSO explores numerous expressions according to how they fit the dataset, and outputs the higher-quality one as the solution of the problem [27], [29]. Fig. 4 presents a simplified example of the DSO framework. Note that for each token, the recurrent neural newtork (RNN) emits a categorical distribution over tokens. A token is sampled, and the parent and sibling of the next token are used as the next input to the RNN. Subsequent tokens are sampled autoregressively until the tree is complete. In this way, the resulting sequence of tokens is the tree's pre-order traversal, which can be used to reconstruct the tree and instantiate its corresponding expression.

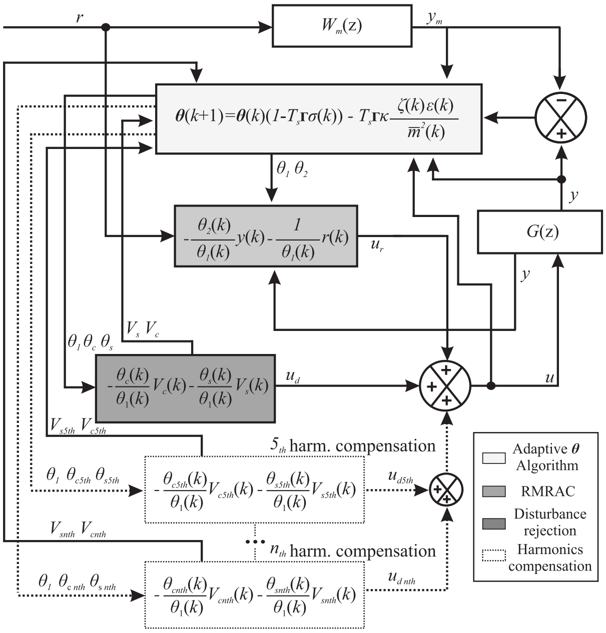

FIGURE 3. **RMRAC with selective harmonics compensation (5^{th} to n^{th}).**

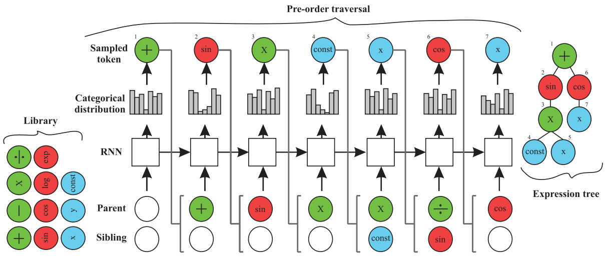

FIGURE 4. **DSO framework example.**

DSO generates a symbolic expression that represents the underlying dynamics of the system being modeled. This expression can provide valuable insights into the behavior of the system and can be interpreted by experts in the field or even by other algorithms, avoiding the interpretability problem of most learning-based techniques [27]. Additionally, DSO tends to be less prone to overfitting than fitting a neural network as in a standard regression problem. Overfitting occurs when a model is too complex and fits the training data too closely, leading to poor performance on new data. This is avoided because DSO's output is a mathematical expression easy to inspect and to find corner cases, as well as to implement using simple mathematical operators. The application of DSO for predicting the math expression of the grid voltages can therefore provide the following advantages:

1) The symbolic expression generated by DSO can be easily interpreted and used to gain insights into the behavior of the power grid. This can be particularly useful in understanding the impact of different factors on grid performance, such as weather conditions, time of day, and other factors that may affect the behavior of the grid; 2) The symbolic expression generated by DSO can be used to generate forecasts of the grid voltages at the PCC, which can help improve the efficiency and stability of the converter. By accurately predicting the behavior of the grid, the converter can respond more quickly and effectively to changes in the grid, which can help maintain power quality and stability; 3) To take advantage of the symbolic expression generated by DSO, the control structure of the converter can be designed to incorporate feedback based on the predicted grid voltages. For example, an adaptive control system can use the predicted grid voltages to adjust itself to perform a selective harmonics compensation on regulated currents, adjusting the output of the converter and ensuring an adequate tracking of currents with acceptable THD, even in the face of challenging grid conditions.

The choice between DSO and neural networks depends on the specific problem being addressed, and a thorough analysis of both techniques should be performed to determine the most appropriate approach. By following this method, the final outcome of the DSO is an equivalent mathematical expression, which in this application can be used to evaluate the voltage distortion and grid behavior in order to give feedback to the DC-AC control structure. As previously noted, real-time learning-based techniques tend to require high computational demand. Thus, this procedure proposes to use DSO in windows of time every few minutes. To accelerate the DSO outcomes, cloud-based computing can be implemented to significantly reduce the time that the DSO algorithm takes to identify the grid voltage main harmonics and feed back to the control system the information about which specific harmonics should be compensated for by the adaptive structure. The cloud-based implementation was not developed for this version of the manuscript, but it constitutes a possible future work direction in this topic. As such, it is an evaluation that is performed offline, feeding the controller structure back to be reorganized properly as soon as the regression is done. Fig. 5 presents a DC-AC converter schematic considering an adaptive control structure with DSO feedback.

The pseudo-code presented in Algorithm 1 can be considered for the RMRAC-based control structure taking advantage of DSO grid-voltages prediction for GCCs.

V. RESULTS

In order to compare the results obtained with the proposed adaptive control structure, the VSI grid-injected current was regulated by an RMRAC, an RMRAC-ASTSM structure, and the RMRAC with DSO feedback. The RMRAC-ASTSM structure was presented in [12], while the RMRAC's mathematical development was shown in Section III-A. Regarding comparing adaptive with classical controllers, it is worth noting that a direct comparison, in this case, may not provide a like-for-like assessment, given the inherent advantage of the adaptive controller in facing a broader range of scenarios and disturbances. Such a comparison could inadvertently present an oversimplified perspective, possibly leading to an unfair advantage in favor of the adaptive controller [6].

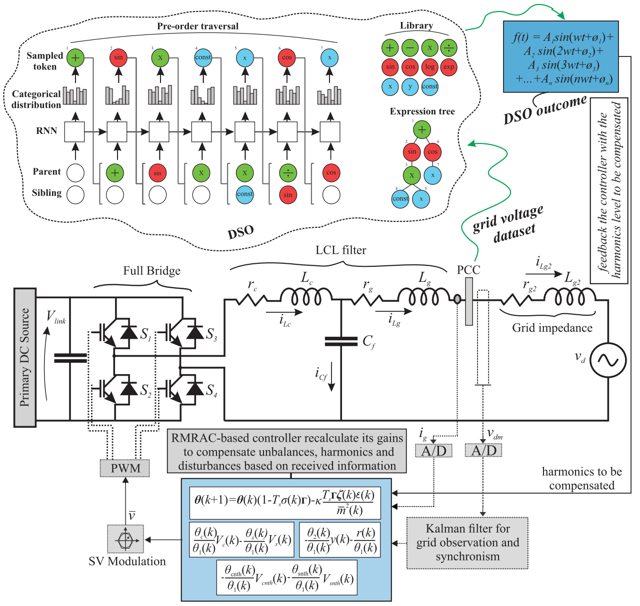

FIGURE 5. **RMRAC with DSO for grid-injected currents control of a single-phase DC-AC converter.**

A. EXPERIMENT CONFIGURATION

The results were obtained in a controller-hardware-in-the-loop (C-HIL) environment. For obtaining the results, a Typhoon HIL 604 was used to run the converter dynamics, and the control algorithms were implemented in a TMS320F28335 DSP. By this means, the control algorithms presented A/D readings, signal conditioning, grid-syncing using KF-PLL, control law calculations, space vector modulation, and PWM generation for the full-bridge switches. So, the same code that is implemented in the C-HIL environment can be used for the real prototype. The switching frequency is 5040 Hz and the sampling frequency is also of 5040 Hz. The DC bus voltage was set to 400 V, while the grid voltage was 120 V, considering 3% and 2% of the 5^{th} and 7^{th} harmonics, respectively. Furthermore, the normalized grid voltage was estimated using the KF-PLL algorithm from [31], and the GCC full bridge switches were updated with the control action $u(k)$, synthesized by the space vector modulation proposed by [32]. The steps of the realized experiment follow the routine: (i) When the converter is grid-synced (there is $t = 0$ s), the peak current reference is set to 10 A (33% load) and it remains with this amplitude until $t = 0.2$ s. (ii) At $t = 0.2$ s, the current peak reference is updated to 20 A (66% load). (iii) When $t = 0.5$ s, the current peak reference is set to 30 A (full load). (iv) At $t = 1.5$, a disturbance is imposed in the grid in which a 5 mH inductor is added in series with the L_g inductor of the LCL filter (please refer to Fig. 1 and

Algorithm 1 Pseudo-Code of the Control Algorithm Using RMRAC With DSO Applied for GCCs

```
initialization;
read DC link voltage;
read currents and voltages at PCC;
update the grid-sync algorithm: observing grid
  voltage from Kalman filter [31];
if converter can be connected to the grid then
    connect to the grid;
    while connected to the grid do
        regulate DC link voltage;
        generate current reference amplitude using
          normalized values from Kalman filter [31];
        if grid prediction from DSO arrived then
            check grid condition;
            if check for harmonics on the DSO
              expression then
                recalculate the adaptive gains and
                  control laws considering selective
                  harmonics compensation: Equations
                  (20)-(21),(9)-(16);
                space vector modulation [32];
            else
                wait for new grid prediction;
            end
        else
            keep standard operation:
              Equations (6)-(21);
            space vector modulation [32];
        end
    end
else
    keep waiting for grid-sync: observing grid voltage
      from Kalman filter [31];
end
```

Fig. 5). From this moment on, the grid is very weak, with a short-circuit ratio (SCR) < 3. Note also that the grid voltage is also severely distorted (emulating a less-inertia power grid scenario). (v) When $t = 3$ s, the GCC is disconnected from the grid.

The adaptive control structures were designed using the same reference model, shown in (19). Also, the RMRAC and the RMRAC with DSO feedback were tuned with the following design parameters: $\kappa = 2500$, $\boldsymbol{\Gamma} = 1$, $M_0 = 10$, $\sigma_0 = 0.18$. For the RMRAC structure, some restrictions emerge from [34], but according to [22] and [23], the following limitation should be observed: $\boldsymbol{\Gamma}\kappa T_s < 20$. As previously mentioned, it is important to highlight that the design constraints obtained with the RMRAC structure are the same for RMRAC with DSO feedback, since the new feature in this controller is the selective harmonics compensation. The addition of reconfigurable harmonics rejection terms does not harm the stability of the adaptive controller if the adaptive algorithm is stable and the controller is robust to matched and unmatched dynamics. Also, the normalized voltages of the harmonics were obtained with the Kalman filter algorithm from [31], which is limited and stable. The RMRAC-ASTSM structure presented the following design values: $\kappa = 2500$, $\boldsymbol{\Gamma} = 1$, $M_0 = 10$, $\sigma_0 = 0.18$, $k_1 = 1$ and $k_2 = 0.0001$. These parameters were obtained according to [12]. The adaptive gains vector $\boldsymbol{\theta}$ for the RMRAC was $\boldsymbol{\theta}_{(0)}(k) = [\,1\ \ -1\ \ 0.01\ \ 0.5\,]$, while for the RMRAC-ASTSM structure it was $\boldsymbol{\theta}_{(0)}(k) = [\,1\ \ -1\ \ 0.01\ \ 0.5\ \ -0.004\,]$. Finally, the proposed RMRAC-based controller with DSO feedback for selective harmonics compensation had $\bar{\boldsymbol{\theta}}_{(0)}(k) = [\,1\ \ -1\ \ 0.01\ \ 0.5\ \ 0.25\ \ 0.65\ \ 0.17\ \ 0.36\,]$.

B. DSO CONFIGURATION

The DSO was implemented for regression. The dataset considered is the grid voltage for a single-phase DC-AC converter with the parameters presented in Section II. The schematic is the same as that depicted in Fig. 1 and Fig. 5. Then, the grid voltage was measured at the PCC in a Simulink simulation, where the voltage presented 3% and 2% of the 5^{th} and 7^{th} harmonics, respectively. The considered evaluated expressions with DSO have 2 axes, corresponding to x and y, x being the time and y being the corresponding sinusoidal amplitude from the x axis. Then, the DSO algorithm evaluated expression (fitness function) has the form $y = f(x)$.

The DSO algorithm is open-source, and the implemented version is release v3.0 found on github. The algorithm was not modified from the release version, and it was tuned considering the neural-guided genetic programming population-seeding controller. For setting up the optimization algorithm, a virtual environment using Anaconda was created, and Python 3 was used for running the configuration script that starts the optimization. The number of generations was 30, and a crossover of 0.5% was considered as well as a 0.5% mutation rate. The total number of samples of the dataset (grid voltage read at the PCC) was 4000000, with a batch size of 1000. The learning rate was set to 0.0025 and the entropy weight was 0.03, while the gamma was 0.7. Also, the epsilon considered for the run was 0.05. The threshold for early stopping criteria was 1e-12, but the early stopping criteria was disabled, aiming for a scenario in which we do not correctly know the data expression. The maximum expression size was 40 tokens, and the minimum was 2.

The token list considered for the DSO run was [‘+’ ‘-’ ‘*’ ‘/’ ‘sin,’ ‘cos,’ ‘180,’ ‘π’ ‘60,’ ‘377,’ ‘1131,’ ‘1885,’ ‘2639,’ ‘0.5,’ ‘1.0,’ ‘1.8,’ ‘2.0,’ ‘3.0,’ ‘3.6,’ ‘4.0,’ ‘5.0,’ ‘5.4’]. Note that the token list should be defined by the designer, and insofar as more favorable expressions are included in the token list, the convergence time tends to be reduced. Thus, since we know the dataset (grid voltage with fundamental frequency of 60 Hz), it is possible to insert some constant tokens that reduce the optimization time. The included constant numbers (such as 377 ($2\pi f$), 1131 ($3\pi f$), 1885 ($5\pi f$) were chosen because we expected them to be present in the ground-truth equations in this domain. For the configurations presented,

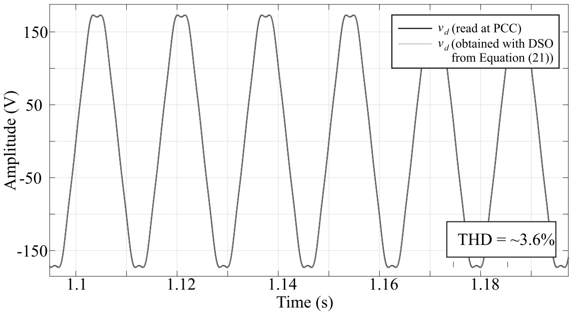

FIGURE 6. **Grid-voltage measured at PCC and grid voltage obtained with DSO.**

the usual time to complete one epoch is around 2 seconds, while convergence is usually achieved around epoch 240. In this scenario, the total time for running the DSO was around 6 minutes.[1] It is important to highlight that this execution time can be drastically reduced if a cloud-computing method or a superior computer is considered for running the algorithm. However, a standard computer was used for this application, but the cloud-based implementation can be a future work to reduce the technique's computational burden.

The best fitness function found from the DSO algorithm is the following:

$$180.0 \cdot sin(377.0 \cdot x_1) - 5.4 \cdot sin(1885.0 \cdot x_1) + 3.6 \cdot sin(2639.0 \cdot x_1). \tag{22}$$

Observe in the argument of trigonometrical functions that the expression obtained with DSO identifies the presence of the 5^{th}-order and 7^{th}-order harmonics. This information is fed back into the adaptive control algorithm in the DSP by means of GPIOs in order to enable the selective harmonics compensation and inform the controller of which harmonics should be compensated according to the grid behavior.

Fig. 6 presents the waveform of the corresponding grid voltage read at the PCC using the C-HIL environment, v_d, as well as that obtained with DSO. According to Fig. 6, it is possible to see that both waveforms are very close. Thus, the DSO could properly obtain an equivalent mathematical expression that is accurate to the dataset. Moreover, note the low-frequency distortion in the voltage coming from the 5^{th} and 7^{th} harmonics of the fundamental frequency of the grid (60 Hz), as previously discussed. The THD of the grid voltage (dataset) was 3.6% and that from DSO was around 3.64%.

C. ADAPTIVE CONTROLLERS COMPARISON

Fig. 7 presents the regulated current (i_g) obtained by RMRAC, RMRAC-ASTSM, and RMRAC with DSO feedback. See at the top of Fig. 7(a) -(f) the whole experiment, with the grid synchronization instant, two load steps, and the change in the weak behavior from strong to very weak (same steps presented in Section V-A). Consider Fig. 7(a),(b) and (c), which present the overview of steady-state currents for the RMRAC, RMRAC-ASTSM, and RMRAC with DSO feedback, respectively. These results are measured with the converter already facing a very weak grid scenario (SCR $<$ 3) and with the grid voltage containing severe 5^{th} and 7^{th} harmonics. It is possible to observe that the adaptive control structures keep the current regulated and there is no sign of instability. However, a low frequency distortion can be seen in the RMRAC and RMRAC-ASTSM, which is not observed in the proposed structure. When observing the same currents in detail, it is possible to see in Fig. 7(d), (e) and (f) an improved waveform in the RMRAC structure with selective harmonics compensation obtained with the feedback from the DSO algorithm. An additional measurement is also performed and is presented in Fig. 7(g), (h) and (i). These results were captured after the inclusion of harmonics in the grid and after convergence of all parameters. The acquisition method in the osciloscope was changed from high-resolution to 16 samples average, in order to better see the differences between the regulated currents. Note that the grid-tied converter is still operating in a very weak grid scenario with the grid voltage distorted by 5^{th} and 7^{th} harmonics. It is possible to clearly see the regulation difference between the RMRAC, the RMRAC-ASTSM, and the RMRAC with DSO. All adaptive gains from all controllers have already converged, but a low-frequency distortion is clearly present in RMRAC and RMRAC-ASTSM structures, which makes sense since there is no feedback for harmonics compensation in those structures. Furthermore, observe that in the RMRAC with DSO, regulated currents have a small low-frequency imperfection in the positive semi-cycle, but the overall shape of the waveform is close to a perfect sinusoidal.

The frequency for capturing the internal signals in the DSP was 630 Hz, i.e., one sample is saved for each 8 samples processed. This was developed due to memory limitations in the DSP. However, this frequency is enough to check the behavior and convergence of the internal signals. Fig. 8 presents the regulated current-tracking error (e_1) obtained by RMRAC, RMRAC-ASTSM, and RMRAC with DSO feedback for the 3 s experiment. It is possible to observe that RMRAC with DSO feedback presented the smallest values of current-tracking error. The computed RMS value for e_1 in steady state at full load considering a strong grid (from 1 s to 1.5 s) was 2.0278 A, 1.9725 A, and 1.5783 A for the RMRAC, RMRAC-ASTSM, and RMRAC with DSO structures, respectively. In addition, the computed RMS value for e_1 in steady state at full load considering a very weak grid (from 1.9 s to 3 s) was 0.6037 A, 0.6201 A, and 0.4909 A for the RMRAC, RMRAC-ASTSM, and RMRAC with DSO structures, respectively.

Fig. 9 presents the RMRAC control action (u_r) obtained by RMRAC, RMRAC-ASTSM, and RMRAC with DSO feedback. Regarding the control action u_r, it is possible to observe in Fig. 9(a) and Fig. 9(b) that this control action

---

[1] Algorithm implemented in an 11^{th} generation Intel Core i5-11400H, 2.7 GHz, 32 GB RAM considering 6 cores parallelism.

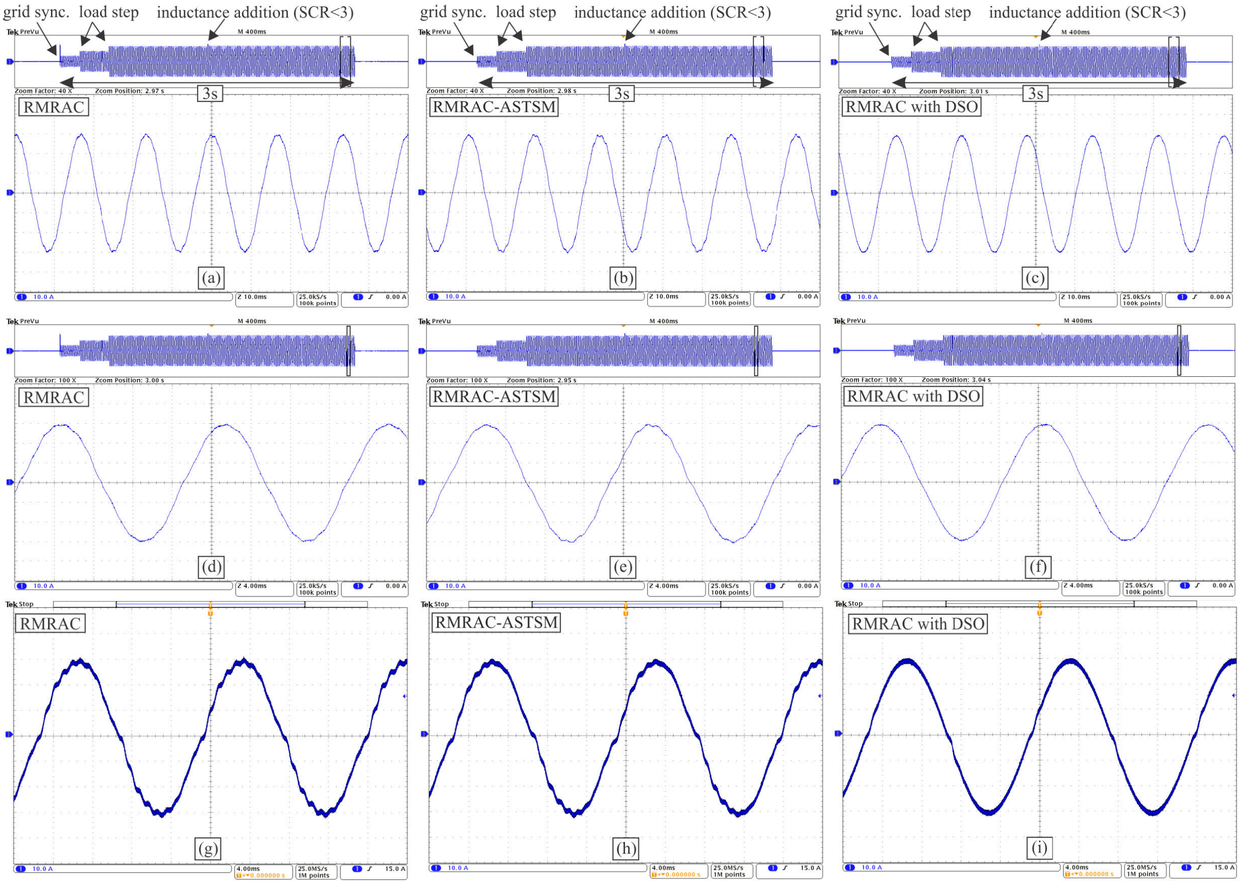

FIGURE 7. **Grid-injected current comparison in a very weak grid scenario, with v_g containing 3% and 2% of the 5^{th} and 7^{th} harmonics. (a),(b),(c) are the overview of the regulated current for the RMRAC, RMRAC-ASTSM, and RMRAC with DSO feedback; (d),(e),(f) detail of the regulated current for the RMRAC, RMRAC-ASTSM, and RMRAC with DSO feedback; (g),(h),(i) Regulated current in a less-inertia power grid (after all parameters convergence).**

is significantly distorted during the experiment. This occurs because with the grid voltage distorted, the current tracking error also tends to present several distortions, and since u_r represents the RMRAC control action related to θ_1 and θ_2 (referring to u_r and i_g), these parameters tend to be very sensitive to distortions, disturbances, and unmodeled dynamics in the plant. However, it is possible to observe in Fig. 9(b) that the RMRAC structure with DSO feedback providing the selective harmonics information presents a better shape and small amplitudes (less control effort) regarding u_r.

Fig. 10 presents the control actions for selective harmonics compensation by RMRAC with DSO feedback. Considering Fig. 10, it can be seen that the control actions are well behaved and actuate during the entire experiment, which makes sense, as the grid voltage is distorted from the grid sync moment. In addition, the control actions are more disturbed during the grid inductance addition instant (very weak grid in $t = 1.5$ s), which is coherent since this parametric variation going abruptly from a strong grid to a very weak grid tends to significantly impact the system behavior and requires the adaptive gains to change and converge to new values.

Fig. 11 presents the adaptive gains vector ($\bar{\boldsymbol{\theta}}$) obtained by RMRAC with DSO feedback. As can be seen, the adaptive gains converge at steady state after the load steps and after the L_{g2} parametric variation (very weak grid) at $t = 1.5$ s. In addition, it is possible to observe that θ_1 and θ_2 (coming from MRAC), as well as θ_c and θ_s (coming from 60 Hz compensation), present a strong dynamic after each disturbance. This behavior is expected since θ_1 and θ_2 are the gains related to the complete control action (u) and the regulated current (y), respectively. Both are sensitive to load steps and parametric variations. Moreover, the gains θ_c and θ_s generate the u_d control action, which tends to dominate the dynamics of complete control action u. Also, Fig. 12 presents a harmonics analysis of the regulated currents for the RMRAC and RMRAC with DSO in a very weak grid with the grid voltage distorted (less-inertia power grid). These harmonics were computed considering the steady state currents presented in Fig. 7(g) and (i). It is possible to observe that the proposed structure outperforms the RMRAC structure without DSO. Note the significant difference in the 5^{th} and 7^{th} harmonics amplitudes, which were compensated for by the

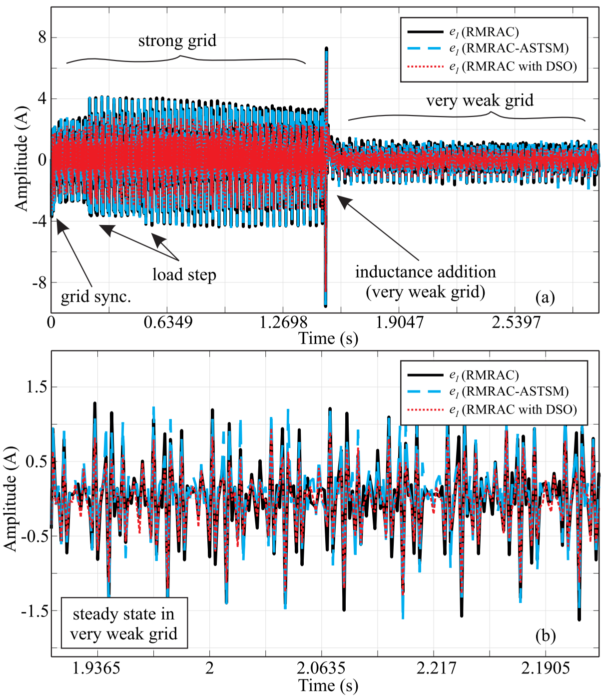

FIGURE 8. Current tracking error (e_1) comparison between RMRAC, RMRAC-ASTSM and RMRAC with DSO feedback. (a) Overall view of the 3 s experiment; (b) detail of the steady state at full load in a very weak grid scenario with v_g distorted.

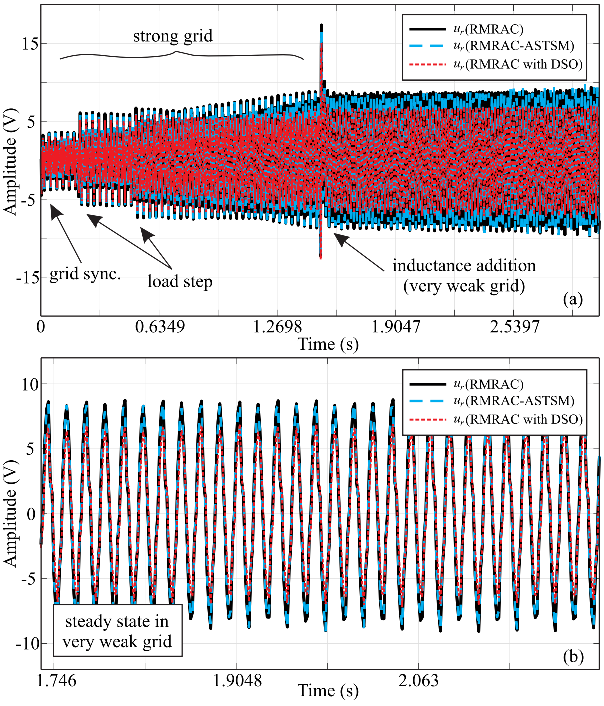

FIGURE 9. RMRAC control action u_r comparison. (a) Overall view; (b) Detail of the control action considering the very weak grid scenario with v_g distorted.

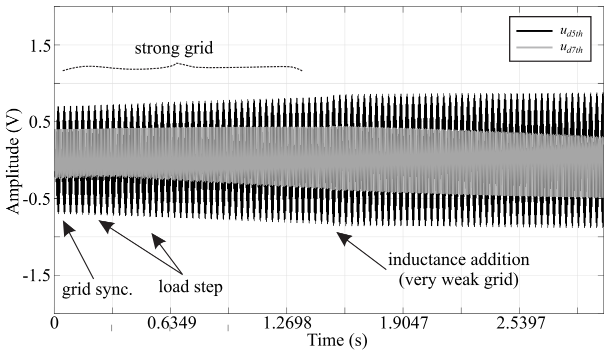

FIGURE 10. Control actions for selective harmonics compensation from RMRAC with DSO. (a) u_{d5th}; (b) u_{d7th}.

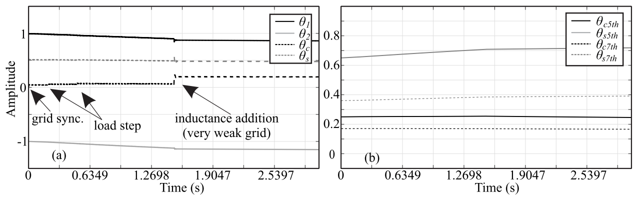

FIGURE 11. Adaptive gains θ. (a) θ_1, θ_2, θ_c and θ_s; (b) θ_{c5th}, θ_{s5th}, θ_{c7th} and θ_{s7th}.

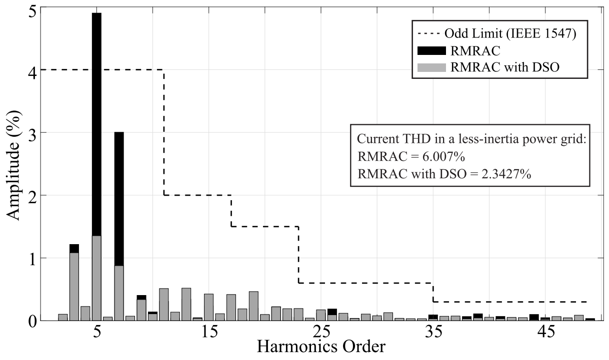

FIGURE 12. Grid injected current harmonic analysis for the RMRAC and the RMRAC with DSO feedback.

active adaptive harmonics compensation fed back by the DSO algorithm. The RMRAC structure does not comply with the IEEE 1547 [14] in terms of individual limits, different from the proposed controller. Moreover, the THD for all structures was computed, and the RMRAC with DSO presented a 2.3427% THD against a 5.3911% and 6.007% obtained by the RMRAC and RMRAC-ASTSM, respectively. Note that IEEE 1547 establishes that the grid-injected current THD should be less than 5%. Hence, for the worst case scenario (very weak grid with v_g distorted), the only structure that meets the standard is the RMRAC with DSO.

Fig. 13 presents an additional experiment regarding the proposed control structure considering sudden voltage drops. This test is carried out in the worst case scenario (very weak grid with 5^{th} and 7^{th} harmonics in v_g). Fig. 13(a) shows the behavior of the controller in current regulation considering a 10% voltage drop in the grid voltage, going from 120 V to 108 V. Observe that the grid voltage is 20 V/1 Vdac, i.e.,

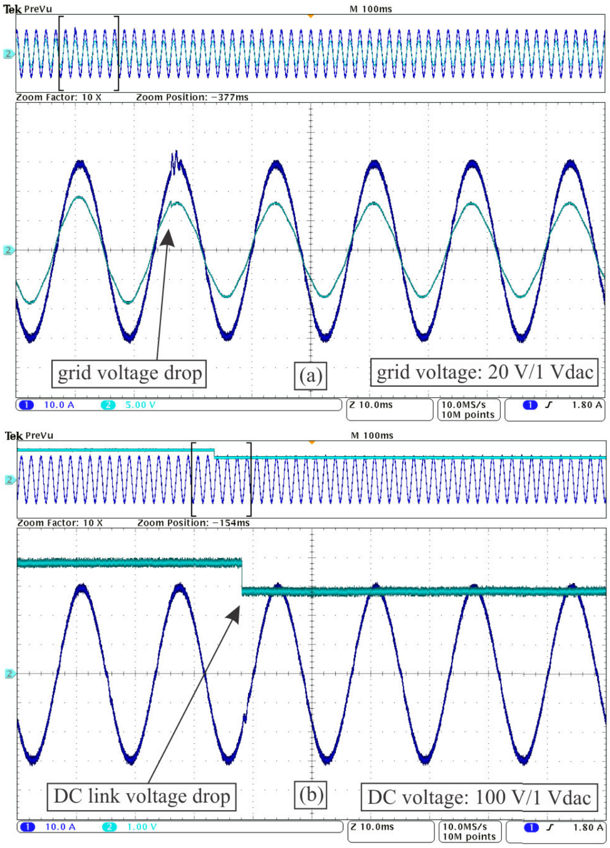

FIGURE 13. **Proposed controller in a sudden voltage drop (very weak grid with v_g distorted scenario). (a) v_g drops 10%; (b) V_{link} drops 25%.**

TABLE 1. **Controllers comparison: summary of main results (best results for each metric are highlighted in bold).**

Controller	i_g THD (SCR<3)	e_1 (SCR>20)	e_1 (SCR<3)
RMRAC	6.007%	2.0278 A	0.6037 A
RMRAC-ASTSM	5.3911%	1.9725 A	0.6201 A
RMRAC with DSO	**2.3427%**	**1.5783** A	**0.4909** A

10 V in the oscilloscope represents a 200 V measurement in the HIL environment. Fig. 13(b) shows the behavior of the controller in current regulation considering a 25% voltage drop in the DC bus voltage (V_{link}), going from 400 V to 300 V. In the same way, note that the V_{link} is 100 V/1 Vdac, i.e., 5 V in the oscilloscope corresponds to 500 V. In both scenarios the controller kept the system stable and well regulated.

Table 1 presents a summary comparison between RMRAC, RMRAC-ASTSM, and RMRAC with DSO for grid-injected current control of the VSI. It is possible to see that the RMRAC structure with selective harmonics compensation obtained with DSO feedback outperformed the other adaptive controllers in terms of tracking performance and grid-injected current THD, as previously discussed. Also, it is important to highlight that the tuning constants and the initial values of $\boldsymbol{\theta}$ were the same for all adaptive control structures. For the tracking errors, the RMRAC with DSO presented up to a 22.17% reduction in e_1 (RMS) when compared with the RMRAC and a 20.84% reduction when compared with the RMRAC-ASTSM. Regarding the grid-injected current THD, the proposed controller presented up to a 61% reduction, going from a THD of 6.007% and 5.3911% to 2.3427%. Also, it is important to highlight that for this application, 2 harmonics were compensated for, but other orders of harmonics can additionally be compensated for, and since the control structure is reconfigurable, the number of compensations as well as the order can be configured according to each application, limited to the memory of the DSP. However, for each compensated component, 2 new adaptation gains arise in each coordinate, which has direct impacts on the controller complexity and consequently increases its real-time computational burden. The main drawback of the proposed controller is the computational burden requested for the DSO algorithm to identify the harmonics to be compensated in the grid, which needs to be executed in windows of time every few minutes. However, if a better computer is dedicated for this task, this time can be drastically reduced to only a few seconds.

VI. CONCLUSION

In this work, a robust model reference adaptive controller with a reconfigurable selective harmonics compensation strategy was proposed and implemented for the current-control loop of a grid-connected converter with an LCL filter. The controller was designed to apply a deep symbolic optimization algorithm to the grid voltage read at the PCC, obtaining the equivalent mathematical expression and feeding it back to the controller with information about which harmonics should be compensated for to improve the efficiency. Hardware-in-the-loop results were presented with the converter operating in both a strong and a very weak grid scenario, with the grid voltage severely distorted (less-inertia power grid). The proposed controller was compared with two other direct adaptive controllers. The proposed structure outperformed the other controllers in terms of tracking error (with a reduction up to 22.17%) and total harmonic distortion of grid-injected currents (2.34% against 5.39% and 6%). The proposed method can be extended to other direct adaptive controllers and topologies, and since the selective harmonics compensation is reconfigurable, it can vary depending on the application, which makes the proposal not unfeasible or unreconfigurable for high-order systems.

ACKNOWLEDGMENT

The authors would like to thank Typhoon HIL© for the research support. Any opinions, findings, and conclusions or recommendations expressed in this material are those of the author(s) and do not necessarily reflect the views of the National Science Foundation.

REFERENCES

[1] B. Zhang, M. Wang, and W. Su, “Reliability analysis of power systems integrated with high-penetration of power converters,” *IEEE Trans. Power Syst.*, vol. 36, no. 3, pp. 1998–2009, May 2021.

[2] W. Su, A. Q. Huang, M. A. Masrur, A. K. Srivastava, T. Bi, and D. Shi, “Special section on power electronics-enabled smart power distribution grid,” *IEEE Trans. Smart Grid*, vol. 13, no. 5, pp. 3851–3856, Sep. 2022.

[3] J. R. Massing, M. Stefanello, H. A. Grundling, and H. Pinheiro, "Adaptive current control for grid-connected converters with LCL filter," *IEEE Trans. Ind. Electron.*, vol. 59, no. 12, pp. 4681–4693, Dec. 2012.

[4] G. G. Koch, C. R. D. Osório, H. Pinheiro, R. C. L. F. Oliveira, and V. F. Montagner, "Design procedure combining linear matrix inequalities and genetic algorithm for robust control of grid-connected converters," *IEEE Trans. Ind. Appl.*, vol. 56, no. 2, pp. 1896–1906, Mar./Apr. 2020.

[5] Q. Liu, T. Caldognetto, and S. Buso, "Stability analysis and auto-tuning of interlinking converters connected to weak grids," *IEEE Trans. Power Electron.*, vol. 34, no. 10, pp. 9435–9446, Oct. 2019.

[6] G. V. Hollweg, P. D. D. O. Evald, R. V. Tambara, and H. A. Gründling, "Adaptive super-twisting sliding mode for DC-AC converters in very weak grids," *Int. J. Electron.*, vol. 110, no. 10, pp. 1808–1833, Oct. 2023.

[7] R. Peña-Alzola, M. Liserre, F. Blaabjerg, M. Ordonez, and Y. Yang, "LCL-filter design for robust active damping in grid-connected converters," *IEEE Trans. Ind. Informat.*, vol. 10, no. 4, pp. 2192–2203, Nov. 2014.

[8] Y. Kim and H. Kim, "Optimal design of LCL filter in grid-connected inverters," *IET Power Electron.*, vol. 12, no. 7, pp. 1774–1782, Jun. 2019.

[9] R. Peña-Alzola, M. Liserre, F. Blaabjerg, R. Sebastián, J. Dannehl, and F. W. Fuchs, "Analysis of the passive damping losses in LCL-filter-based grid converters," *IEEE Trans. Power Electron.*, vol. 28, no. 6, pp. 2642–2646, Jun. 2013.

[10] W. Wu, Y. He, T. Tang, and F. Blaabjerg, "A new design method for the passive damped LCL and LLCL filter-based single-phase grid-tied inverter," *IEEE Trans. Ind. Electron.*, vol. 60, no. 10, pp. 4339–4350, Oct. 2013.

[11] T. Liu, J. Liu, Z. Liu, and Z. Liu, "A study of virtual resistor-based active damping alternatives for LCL resonance in grid-connected voltage source inverters," *IEEE Trans. Power Electron.*, vol. 35, no. 1, pp. 247–262, Jan. 2020.

[12] G. V. Hollweg, P. J. D. D. O. Evald, R. V. Tambara, and H. A. Gründling, "A robust adaptive super-twisting sliding mode controller applied on grid-tied power converter with an LCL filter," *Control Eng. Pract.*, vol. 122, May 2022, Art. no. 105104.

[13] C. K. Duffey and R. P. Stratford, "Update of harmonic standard IEEE-519: IEEE recommended practices and requirements for harmonic control in electric power systems," *IEEE Trans. Ind. Appl.*, vol. 25, no. 6, pp. 1025–1034, 1989.

[14] *Standard for Interconnecting Distributed Resources With Electric Power Systems*, Standard IEEE:1547, 2011.

[15] J. Liu, Y. Miura, H. Bevrani, and T. Ise, "Enhanced virtual synchronous generator control for parallel inverters in microgrids," *IEEE Trans. Smart Grid*, vol. 8, no. 5, pp. 2268–2277, Sep. 2017.

[16] X. Ruan, X. Wang, D. Pan, D. Yang, W. Li, and C. Bao, *Control Techniques for LCL-Type Grid-Connected Inverters*. Berlin, Germany: Springer, 2018.

[17] M. Elkayam and A. Kuperman, "Optimized design of multiresonant AC current regulators for single-phase grid-connected photovoltaic inverters," *IEEE J. Photovolt.*, vol. 9, no. 6, pp. 1815–1818, Nov. 2019.

[18] Y. Guo, H. Sun, Y. Zhang, Y. Liu, X. Li, and Y. Xue, "Duty-cycle predictive control of quasi-Z-source modular cascaded converter based photovoltaic power system," *IEEE Access*, vol. 8, pp. 172734–172746, 2020.

[19] I. Poonahela, S. Bayhan, H. Abu-Rub, M. M. Begovic, and M. B. Shadmand, "An effective finite control set-model predictive control method for grid integrated solar PV," *IEEE Access*, vol. 9, pp. 144481–144492, 2021.

[20] Y. Liu et al., "A novel adaptive model predictive control strategy of solid oxide fuel cell in DC microgrids," *IEEE Trans. Ind. Appl.*, vol. 58, no. 5, pp. 6639–6654, Sep. 2022.

[21] A. Nardoto, A. Amorim, N. Santana, E. Bueno, L. Encarnação, and W. Santos, "Adaptive model predictive control for DAB converter switching losses reduction," *Energies*, vol. 15, no. 18, p. 6628, Sep. 2022.

[22] K. J. Astrom and B. Witternmark, *Adaptive Control*. New York, NY, USA: Dover, 1995.

[23] P. Ioannou and J. Sun, *Robust Adaptive Control*. New York, NY, USA: Dover, 2012.

[24] R. V. Tambara, J. M. Kanieski, J. R. Massing, M. Stefanello, and H. A. Gründling, "A discrete-time robust adaptive controller applied to grid-connected converters with LCL filter," *J. Control, Autom. Electr. Syst.*, vol. 28, no. 3, pp. 371–379, Jun. 2017.

[25] P. J. D. D. O. Evald, G. V. Hollweg, R. V. Tambara, and H. A. Gründling, "A hybrid robust model reference adaptive controller and proportional integral controller without reference model for partially modeled systems," *Int. J. Adapt. Control Signal Process.*, vol. 37, no. 8, pp. 2113–2132, Aug. 2023.

[26] D. M. C. Milbradt, G. V. Hollweg, P. J. D. D. O. Evald, W. B. da Silveira, and H. A. Gründling, "A robust adaptive one sample ahead preview controller for grid-injected currents of a grid-tied power converter with an LCL filter," *Int. J. Electr. Power Energy Syst.*, vol. 142, Nov. 2022, Art. no. 108286.

[27] B. K. Petersen, M. Landajuela, T. N. Mundhenk, C. P. Santiago, S. K. Kim, and J. T. Kim, "Deep symbolic regression: Recovering mathematical expressions from data via risk-seeking policy gradients," 2019, *arXiv:1912.04871*.

[28] T. N. Mundhenk, M. Landajuela, R. Glatt, C. P. Santiago, D. M. Faissol, and B. K. Petersen, "Symbolic regression via neural-guided genetic programming population seeding," 2021, *arXiv:2111.00053*.

[29] M. Landajuela et al., "A unified framework for deep symbolic regression," in *Proc. Adv. Neural Inf. Process. Syst.*, 2022, vol. 35, pp. 33985–33998.

[30] A. Reznik, M. G. Simões, A. Al-Durra, and S. M. Muyeen, "LCL filter design and performance analysis for grid-interconnected systems," *IEEE Trans. Ind. Appl.*, vol. 50, no. 2, pp. 1225–1232, Mar. 2014.

[31] R. Cardoso, R. F. de Camargo, H. Pinheiro, and H. A. Grundling, "Kalman filter based synchronisation methods," *IET Gener., Transmiss. Distrib.*, vol. 2, no. 4, pp. 542–555, 2008.

[32] L. Michels, R. F. de Camargo, F. Botteron, H. A. Grüdling, and H. Pinheiro, "Generalised design methodology of second-order filters for voltage-source inverters with space-vector modulation," *IEE Proc.-Electric Power Appl.*, vol. 153, no. 2, pp. 219–226, 2006.

[33] P. A. Ioannou and P. V. Kokotovic, *Adaptive Systems With Reduced Models*. Berlin, Germany: Springer, 1983.

[34] P. Ioannou and K. Tsakalis, "A robust discrete-time adaptive controller," in *Proc. 25th IEEE Conf. Decis. Control*, Dec. 1986, pp. 838–843.

[35] G. V. Hollweg, P. J. Dias de Oliveira Evald, D. M. C. Milbradt, R. V. Tambara, and H. A. Gründling, "Lyapunov stability analysis of discrete-time robust adaptive super-twisting sliding mode controller," *Int. J. Control*, vol. 96, no. 3, pp. 614–627, Mar. 2023.

[36] R. Lozano-Leal, J. Collado, and S. Mondie, "Model reference robust adaptive control without a priori knowledge of the high frequency gain," *IEEE Trans. Autom. Control*, vol. 35, no. 1, pp. 71–78, Jun. 1990.

GUILHERME VIEIRA HOLLWEG (Member, IEEE) received the B.Sc., M.Sc., and Ph.D. degrees in electrical engineering from the Federal University of Santa Maria (UFSM), Brazil, in 2016, 2019, and 2021, respectively. Currently, he is a Research Investigator and an Adjunct Lecturer with the University of Michigan-Dearborn, USA. His main topics of research are adaptive control theory and applications, nonlinear control, power electronics and motor drives control, and optimization algorithms.

VAN-HAI BUI (Member, IEEE) received the B.E. degree in electrical engineering from the Hanoi University of Science and Technology, Vietnam, in 2013, and the Ph.D. degree in electrical engineering from Incheon National University, South Korea, in 2020. He was an Assistant Professor with the Department of Electrical Engineering, State University of New York (SUNY), Maritime College, USA, from 2022 to 2023. Since August 2023, he has been an Assistant Professor with the Department of Electrical and Computer Engineering, University of Michigan-Dearborn, USA. His research interests include energy management systems, applications of machine learning in smart grids, and operation and control of power and energy systems.

FELIPE LENO DA SILVA received the Ph.D. degree in computer engineering from the University of São Paulo, Brazil, in 2019. He is a Staff Reinforcement Learning Researcher with the Lawrence Livermore National Laboratory, USA, where he has been working, since 2021, applying RL to varied applications. He has published one book and over 50 scientific papers in peer-reviewed venues. His research interests spam across several AI areas and applications, such as reinforcement learning, transfer learning, multiagent systems, power electronics, smart grids, transportation, antibody development, and AI-assisted healthcare. He has organized several workshop series, including the Adaptive and Learning Agents (ALA) Workshop, from 2020 to 2022, and the Latinx in AI workshop at NeurIPS. He was a Guest Editor of *Neural Computing and Applications*.

RUBEN GLATT (Member, IEEE) received the Dipl.-Ing. degree in mechatronics from the Karlsruhe Institute of Technology (KIT), Germany, in 2011, the master's degree in mechanical engineering from Universidade Estadual Paulista (UNESP), Brazil, in 2014, and the Ph.D. degree in computer engineering from the University of São Paulo (USP), Brazil, in 2019. In 2019, he joined the Computational Engineering Division, Lawrence Livermore National Laboratory (LLNL), California, USA, as a Postdoctoral Researcher from which he converted to a Staff Researcher in 2021 and a Senior Staff Researcher in 2022. In 2023, he was named as the Director of the Center of Advanced Signal and Image Sciences, LLNL. He has published in the areas of reinforcement learning, knowledge transfer and multi-agent systems, symbolic optimization, generative model applications, and supervised learning. His research interests evolve around general machine learning applications and autonomous agents.

SHIVAM CHATURVEDI (Member, IEEE), photograph and biography not available at the time of publication.

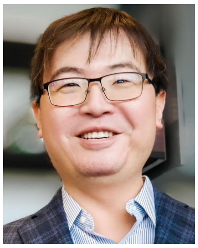

WENCONG SU (Senior Member, IEEE) received the B.S. degree (Hons.) from Clarkson University, Potsdam, NY, USA, in 2008, the M.S. degree from Virginia Tech, Blacksburg, VA, USA, in 2009, and the Ph.D. degree from North Carolina State University, Raleigh, NC, USA, in 2013. He is currently a Professor and the Chair of the Department of Electrical and Computer Engineering, University of Michigan-Dearborn, Dearborn, MI, USA. His current research interests include power systems, electrified transportation systems, and cyber-physical systems. He is a fellow of IET. He received the 2015 IEEE Power and Energy Society (PES) Technical Committee Prize Paper Award and the 2013 IEEE Industrial Electronics Society (IES) Student Best Paper Award. He is an Editor of IEEE Transactions on Smart Grid and IEEE Power Engineering Letters and an Associate Editor of IEEE Access and IEEE DataPort.

• • •